Nanogap Dielectric Spectroscopy for Aptamer-Based Protein Detection

Manu Sebastian Mannoor,[†△] Teena James,[†△] Dentcho V. Ivanov,[†] Les Beadling,[‡] and William Braunlin[‡*]
[†]Microelectronics Research Center, New Jersey Institute of Technology, Newark, New Jersey; and [‡]Rational Affinity Devices, Newark, New Jersey

ABSTRACT Among the various label-free methods for monitoring biomolecular interactions, capacitive sensors stand out due to their simple instrumentation and compatibility with multiplex formats. However, electrode polarization due to ion gradient formation and noise from solution conductance limited early dielectric spectroscopic measurements to high frequencies only, which in turn limited their sensitivity to biomolecular interactions, as the applied excitation signals were too fast for the charged macromolecules to respond. To minimize electrode polarization effects, capacitive sensors with 20 nm electrode separation were fabricated using silicon dioxide sacrificial layer techniques. The nanoscale separation of the capacitive electrodes in the sensor results in an enhanced overlapping of electrical double layers, and apparently a more ordered "ice-like" water structure. Such effects in turn reduce low frequency contributions from bulk sample resistance and from electrode polarization, and thus markedly enhance sensitivity toward biomolecular interactions. Using these nanogap capacitive sensors, highly sensitive, label-free aptamer-based detection of protein molecules is achieved.

INTRODUCTION

Over a decade of rapid advances in nanoscale fabrication technologies is transforming the development of biosensors, and leading to a wide range of potential applications. By the use of miniaturization techniques, sensing elements are now being shrunk to the dimensions of the very biomolecules being sensed. As we describe here for impedance detectors, the unique features of physics on the nanoscale can lead to dramatically enhanced detection sensitivity for nanoscale devices compared to conventional macroscale devices.

Label-free methods for studying biomolecular interactions

The specific detection and precise quantification of protein molecules play an essential role in basic discovery research as well as clinical practice. Most of the high sensitivity methods for studying biomolecular interactions, including protein-ligand binding, require labeling of target or probe molecules with easily detectable substances such as fluorophores (1) or magnetic beads (2). However, for fast, inexpensive molecular detection, label-free methods are preferred, due to the additional sample handling, extra time, and expense associated with the labeling procedure (3). An additional concern is the perturbation of the biomolecular interaction studied by the introduction of large, polarizable, and hydrophobic dye molecules. Among the various label-free signal transduction mechanisms that have been investigated for monitoring biomolecular interactions, capacitive sensors stand out as a promising alternative to conventional fluorescence methods, due to their simple instrumentation as well as their adaptability to multiplexing for high throughput applications (4,5). Nonfaradaic impedance spectroscopy based on capacitive sensors provides a versatile analytical tool for detecting and studying binding events. This versatility reflects the ability of such measurements to explore relaxation processes occurring on an extremely wide range of characteristic times. For such measurements, detection is based on changes in the sensor capacitance or permittivity as a result of probe-target binding. Even though nanogap capacitive sensing is at a much earlier stage than well-developed methods such as surface plasmon resonance and quartz crystal microbalance methods, it seems to have certain intrinsic advantages over these techniques. First, the method should be much less expensive, as it involves simple circuitry that can be manufactured in a straightforward manner, particularly if measurements are made over a limited range of frequencies. Second, it should be more rugged and less prone to misalignment. Finally, due to the small detection volume, it should be highly competitive with these methods in terms of sensitivity. Consequently, it seems self-evident that further characterization and exploration of the method is warranted. This study represents a step in that direction.

Impedance spectroscopy

Impedance or dielectric spectroscopy is a useful analytical tool for studying the structure and dynamics of polyelectrolyte solutions. Its ability to investigate relaxation processes occurring over an extremely wide range of characteristic times (roughly from 10^{-12} s to 10^{3} s) makes it a versatile tool for revealing information about electron transfer, atomic

Submitted July 16, 2009, and accepted for publication October 26, 2009.

[△]Manu Sebastian Mannoor and Teena James contributed equally to this work.

*Correspondence: bbraunlin@rationalaffinity.com

Manu Sebastian Mannoor's present address is Dept. of Mechanical and Aerospace Engineering, Princeton University, Princeton, NJ 08544.
Teena James' present address is Dept. of Chemical and Biomolecular Engineering, The Johns Hopkins University, Baltimore, MD 21218.

Editor: Kathleen B. Hall.

0006-3495/10/02/0724/9 $2.00

doi: 10.1016/j.bpj.2009.10.042

bonds, and molecular motions in polymer solutions (6,7). The characteristic timescale ranges from 10^{-12} s for electrons, 10^{-9} s for atomic bonds, to 10^{-3} s for molecular motions. Therefore, when an oscillatory field excites molecules in a sample they respond differently depending on the frequency. Large-scale changes that occur during target binding to nucleic acid are likely to be revealed during the low frequency response, because it is in the low frequency regime where perturbations in nucleic acid conformation and in the ionic environment around the nucleic acid are likely to be most pronounced.

The dielectric response of DNA solutions has been well studied (8–12). The dielectric relaxation of nucleic acid solutions is typically divided into three different frequency regions: α (near DC to a few kHz frequency range), β (~1 MHz to 1 GHz), and γ (>1 GHz). Among these the α relaxation reflects the migration of counterions over the charged oligonucleotide sequences and hence is closely related to the electrochemical double layer at the vicinity of the electrodes. The impedance due to the double layer dominates the measured capacitance at low frequencies (<1 kHz) and may mask the dielectric property changes resulting from the binding of target to the nucleic acid.

Conventional capacitive biosensors: limitations

Although several configurations of capacitive biosensors have been reported in the literature, their success as reliable biosensing devices has been limited. One major concern is that a strong polarization in the vicinity of the electrodes can result in a large impedance due the electrical double layer that can in turn dwarf dielectric changes due to biomolecular interactions. Also, the aqueous (electrolytic solution) samples usually display a very high ionic electrical conductivity resulting in a large frequency-dependent dielectric dispersion. This parasitic effect associated with the conductivity of the buffer solution in fact masks the dielectric relaxations of interest associated with the biomolecules in the sample. Both of these effects are more pronounced in the low frequency tail of the impedance (dielectric) spectrum. As a consequence, traditional impedance spectroscopic measurements have generally focused on higher frequencies. Unfortunately, at higher frequency, sensitivity toward biomolecular interactions is reduced because resistive contributions dominate over capacitive, and the applied excitation signals are too fast for the charged biomacromolecules to respond (13,14). Proposed methods for minimizing these effects do not lend themselves to biomolecular sensing applications (15,16).

In an effort to address these limitations, we report a nanogap capacitive sensor with an electrode separation of 20 nm. The use of this nanoscale electrode separation provides enhanced sensitivity to molecular interactions, which was not attainable previously with macro- or even microscale devices. The reduced electrode separation of nanogap devices results in the overlapping of the electrical double layers and decreases the potential drop across the electrode spacing, and thereby facilitates dielectric measurements at low frequency (17).

Advantages of aptamer-based sensing

The detection of protein molecules using immobilized antibodies has been used for a wide range of applications for more than three decades (18). However, there are certain limitations associated with antibody based sensing. The loss of activity of surface immobilized antibodies is a major drawback, making the regeneration of antibody surfaces extremely difficult (19). The maintenance of the specificity and integrity of antibody functions requires mild solution conditions. The use of nucleic acid aptamers as sensor recognition elements overcomes many of the shortcomings of antibody functionalized sensors, and is currently a very active area of research (5,20,21). The ability to regenerate the functionality of immobilized aptamers is one of its most attractive features. As aptamers are oligonucleotide sequences, they can be subjected to repeated cycles of denaturation and renaturation. Immobilized aptamers can withstand extreme conditions of temperature and salt concentrations, without being damaged, which increases the shelf life of these sensors. Another major advantage of the aptamer based sensors is the availability of well-developed immobilization chemistries for the oligonucleotide sequences to various sensor surfaces (22). In our experiments, aptamer sequences modified with thiol groups are used for the functionalization of gold nano-capacitive electrodes. The thrombin aptamer is particularly well-studied and is generally the first choice as a proof-of-principle for aptamer-based sensing methods. In contrast to most other known aptamers, which have a high degree of conformational flexibility, the thrombin aptamer forms a well-defined quadruplex structure, that is essential for specific binding to α-thrombin (23–25).

Theory and detection scheme

Nanogap capacitive sensor

Detection is based on changes in sensor capacitance (relative permittivity) due to variations in the dielectric properties of the Debye layer resulting from the binding of protein molecules to immobilized DNA aptamer probes. The double layer capacitance formed by the accumulation of counterions near the electrode surface is extremely sensitive to the changes in the dielectric and charge environment at the electrode/electrolyte interface and reveals much information about the aptamer-protein interactions. According to elementary theory, the characteristic length of this diffuse double layer of charges (Debye layer) is given by the Debye length. Depending on the ionic conditions, the use of a capacitive element with nanometer scale electrode separation can result in a significant overlap of the double layers of the two

electrodes, thereby confining them to occupy a major fraction of the dielectric volume (17). This dielectric confinement decreases the potential drop across the electrodes and thus facilitates dielectric measurements at low frequencies. Another factor that may reduce the potential drop across the electrodes is the long-range ordering of water molecules and ions within the confined space of the nanogap. This ordering could significantly reduce the ability of the ions to form gradients on the timescale of the AC signal, particularly at higher frequencies.

A theoretical model to evaluate the electrical potential distribution in an overlapped electrical double layer region was first developed by Verwey (26), based on the Gouy-Chapman electrical double layer theory. For simplicity of analysis the Verwey-Overbeek model was developed for an overlapped double layer field between two infinitely large flat electrodes that have the same surface potential.

For infinitely large electrodes, the electrical double layer field between them is one dimensional. Under these circumstances, and with the additional assumption of a 1:1 electrolyte, the Poisson-Boltzmann equation is given by

$$\frac{d^2\psi}{dx^2} = \frac{2en^0}{\varepsilon}\sinh\left(\frac{e\psi}{k_bT}\right), \tag{1}$$

where x is the distance from the electrode surface, ψ is the electrical potential, e is the elementary electronic charge, n^0 is the bulk ion concentration, ε is the bulk dielectric constant, k_b is Boltzmann's constant, and T is the temperature.

In the Verwey-Overbeek model of the overlapped electrical double layer fields (27) the Poisson-Boltzmann equation was applied to the system with the following boundary conditions:

$$\psi|_{x=0} = \psi_0 \tag{2}$$

and

$$\frac{d\psi}{dx}|_{x=b} = 0, \tag{3}$$

where ψ_0 indicates the electrical potential at the surface, and where $2b$ is the separation between the electrodes. If ψ is small, and $e\psi/k_bT < 1$, the right-hand side of Eq. 1 can be simplified by using the approximation, $\sinh x \approx x$. This simplification is referred to as the Debye-Hückel approximation.

Therefore, Eq. 1 can be written as

$$\frac{d^2\psi}{dx^2} = \kappa^2\psi, \tag{4}$$

where κ is defined as

$$\kappa = \left(\frac{2e^2n^0}{\varepsilon k_bT}\right)^{\frac{1}{2}}. \tag{5}$$

κ is referred to as the Debye-Hückel parameter. $1/\kappa$ is the Debye length, which represents the characteristic thickness of the electrical double layer. Equation 4, together with the boundary conditions, Eqs. 2 and 3 can be solved and the solution predicts the potential distribution in the overlapped double layer region as follows:

$$\psi(x) = \psi_0\frac{\cosh(\kappa(b-x))}{\cosh(\kappa b)}. \tag{6}$$

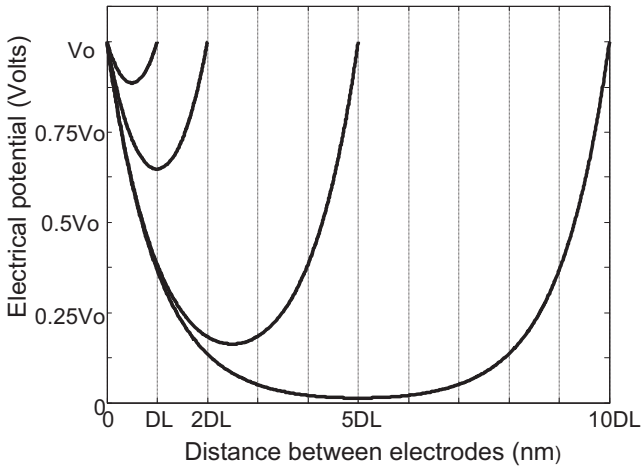

FIGURE 1 Calculated distribution of the electric potential between capacitive electrodes when the position of the second electrode is varied along the x axis with respect to the first electrode. The first electrode is fixed at the position of the y axis ($x = 0$) and the second electrode is moved away from the first electrode along the x axis. The potential distributions for the positions of the second electrode at $x =$ DL, $x = 2$ DL, $x = 5$ DL, and $x = 10$ DL are shown, where DL $= 1/\kappa$. As illustrated in the figure, the potential drop across the double layers is minimized when the separation between the electrodes approaches the width of the electrical double layers (Debye length, $1/\kappa$). This effect reduces the contribution of the double layer impedance to the measured impedance and hence eliminates the so called "electrode polarization effect" in the low frequency dielectric spectrum.

The electrical potential distribution in between the capacitive electrodes were simulated using MATLAB (The MathWorks, Natick, MA) and are illustrated in Fig. 1. The graph shows the variation in the electrical potential distribution between the capacitive electrodes when one of the electrodes is fixed at the position (at $x = 0$) and the second electrode is moved away from the fixed electrode along the positive direction of the x axis. Shown in this figure are calculated potential distributions for capacitive architectures with $2b\kappa = 1$, 2, 5, and 10, where $2b$ is the separation between the electrodes and DL $= 1/\kappa$ is the width of the electrical double layer (Debye length). If $2b$ is equal to 20 nm, then these would correspond to solutions with ionic strengths of 0.178 mM, 0.72 mM, 4.46 mM, and 17.8 mM, respectively.

The graph shows that when the separation between the capacitive electrodes is comparable to or smaller than the electrical double layer, the potential difference between the electrode surface and the middle plane of the sample solution is reduced, which implies that the potential drop across the electrical double layer is minimized as the double layers interact. This calculation indicates clearly that as the

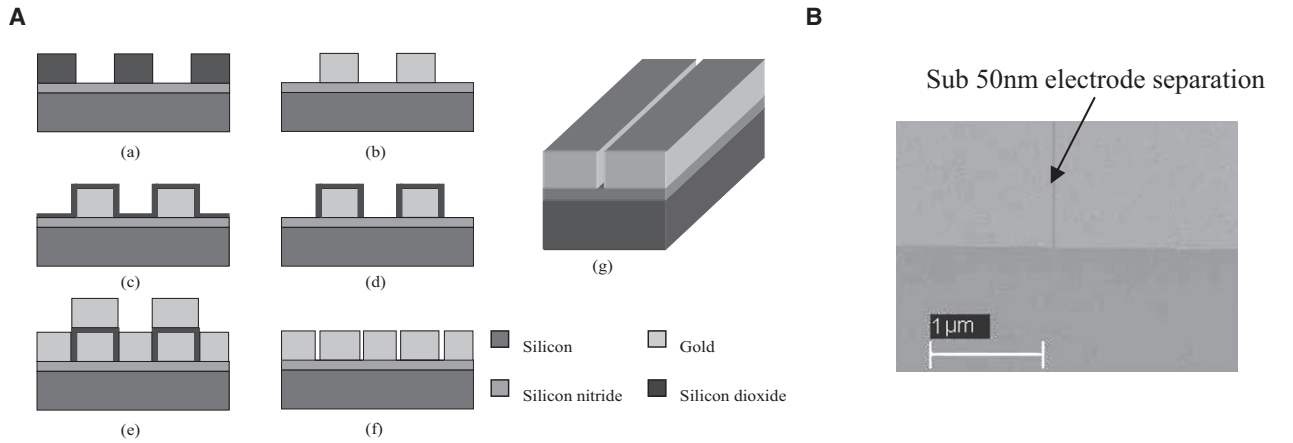

FIGURE 2 (*A*) Schematics of the fabrication process flow: (*a*) photo resist spacers are patterned; (*b*) gold electrodes formed by sacrificial method; (*c* and *d*) deposition and patterning of SiO_2 for nanometer spacing; (*e*) deposition of gold; (*f*) SiO_2 spacer removal; (*g*) a nanogap capacitive sensing structure. (*B*) Electron microscopic image of the Au electrodes with nanoscale separation.

electrode separation is reduced the effect of the electrical double layer impedance on the applied excitation signal is minimized.

MATERIALS AND METHODS

Materials

α-Thrombin aptamers modified with thiol linkers (5′-GGT TGG TTT GGT TGG TTT-$(CH_2)_3$SH-3′) were used for the specific binding experiments. This aptamer differs in two ways from the well-studied 15-mer thrombin aptamer (25). First, it has a TTT tail. This tail allows the aptamer to extend out from the surface of the monolayer, to minimize steric hindrance between the self-assembled monolayer (SAM) surface and the thrombin protein. Second, the central TGT sequence of the original aptamer is changed to a TTT sequence in this aptamer. We have determined that this change has only a modest effect on thrombin binding, but allows a higher degree of selectivity in chromatographic applications (unreported results). Most significantly, the change from TGT to TTT does not hinder the ability of the aptamer to take on the G-quadruplex structure necessary for thrombin binding. Another oligonucleotide, (5′-GTG TGT GTG TGT GTG TTT-$(CH_2)_3$SH-3′) also modified with the thiol linker was used for control experiments. Although this molecule has the same base composition as the thrombin aptamer, because it has no neighboring pairs of guanines it is incapable of forming the quadruplex structure necessary for specific binding, and hence does not function as an aptamer. The DNA molecules used for the experiments were purchased from IDT (Integrated DNA Technologies, Coralville, IA). α-thrombin samples were purchased from Haematologic Technologies (Essex Junction, VT). Lysozyme and the buffer solution 20× SSC (3.0 M sodium chloride + 0.3 M sodium citrate) were purchased from Sigma-Aldrich (St. Louis, MO). The chemicals and other materials used for microfabrication of the device were obtained from the Microfabrication Center at the New Jersey Institute of Technology.

Nanogap sensor fabrication

The most critical parameter for enhancing sensitivity by eliminating the electrode polarization effect is the nanometer separation between the capacitive electrodes. The desired separation of <50 nm is difficult to achieve with conventional lithographic techniques (11). To overcome the resolution limit, we have used a sacrificial layer process, where the thickness of the SiO_2 spacer film determines the electrode separation. The process steps are schematically indicated in Fig. 2.

In the first process step, 500-nm thick silicon nitride is deposited on the smooth side of a polished <100> Si wafer followed by the patterning of 1-μm thick photo resist spacers to act as the sacrificial layer for the formation of the first set of Au electrodes. Gold electrodes are deposited using E-beam evaporation under ultra high vacuum conditions. The selective removal of the photo resist sacrificial layer defines the first set of Au electrodes. In the next step, a very thin and uniform layer of SiO_2 is deposited using plasma enhanced chemical vapor deposition, to form the nanometer spacers between the electrodes. A second layer of 1 μm gold metallization is applied using E-beam evaporation. The Au electrodes are planarized by chemical mechanical polishing and finally the SiO_2 spacer film between the gold electrodes is selectively etched off using HF.

The deposited silicon nitride layer acts as an etch stop during this process and also serves as an isolator between the gold electrodes and the Si wafer. The use of deposited oxide thin film to define the separation between gold electrodes allows the fabrication of capacitive structures with electrode separations lower than the resolution limit of optical or e-beam lithography.

The electrodes obtained by this procedure measured 20 nm across the gap, and were 1 μm deep and 40 μm long.

Oligonucleotide immobilization as part of a mercaptohexanol monolayer

Before the immobilization procedure the structure was cleansed using acetone, isopropanol, and deionized water. Single stranded probe DNA aptamer sequences premodified by the thiol linker (**5′-GGT TGG TTT GGT TGG TTT/3-$(CH_2)_3$SH-3′**) were coimmobilized with mercaptohexanol (MH) on the gold electrodes using a concentration of 10 μM oligomer in the presence of 1 mM MH in 0.5× SSC buffer (75 mM sodium chloride + 7.5 mM sodium citrate). Control oligomer sequences were coimmobilized in a similar manner. By taking advantage of the high affinity of sulfur atoms to gold substrate, the DNA molecules are chemically assembled as part of the MH monolayer onto the gold surface from the solution (28). The <111> crystal orientation of gold that is obtained by thin film deposition provides an optimum substrate for the formation of such monolayers.

Measurement procedure

All measurements were made at room temperature. The dielectric property changes due to hybridization were probed using a Fast-Fourier transform spectrum analyzer. The dielectric properties were investigated over a frequency range of 10 Hz to 100 kHz, with 0V DC bias and 20 mV AC signals using an SR 785, 2-channel dynamic signal analyzer. A Lab View program was used to collect and record data through a GPIB interface. An

external Op-Amp amplifier circuit is used to further minimize the noise. A MATLAB program was used to analyze the raw data to obtain the relative permittivity and the dielectric loss from the signal analyzer output. The electrical contacts and the functioning of the entire system including the capacitive element were verified by measuring the dielectric spectrum with air and deionized (DI) water between the electrodes.

To monitor the formation of the biorecognition layer, measurements were taken before and after aptamer immobilization. After immobilization, α-thrombin solution was added on the sensor surface. After a short incubation time, the variation of the dielectric spectrum was recorded. To monitor the exact response of the sensor toward the bound protein, the measurement was taken after the removal of unbound proteins by washing. As a first control experiment, the above experimental procedure was repeated with lysozyme, a positively charged protein that does not bind specifically to the α-thrombin aptamer. The interaction of α-thrombin molecules to a control oligomer that is unable to form the G-quadruplex binding conformation is carried out as a second control measurement. Each step of the aptamer and control oligonucleotide immobilization and the target binding was characterized by dielectric spectroscopic measurements conducted on the nanogap capacitive electrodes.

RESULTS

The results of the dielectric spectroscopic measurements with air and DI water between the capacitive electrodes of the nanogap sensor are shown in Fig. 3. The response of the sensor to various concentrations of buffer solutions is shown in Fig. 4 *A*. For comparison, in Fig. 4 *B* we show frequency-dependent relative permittivity results for the same buffer solutions for a macroscale interdigitated capacitive sensor (4) with a separation between electrodes of 100 μm. The results shown in Fig. 4 *B* are in substantial agreement with results that have been reported in the literature (29).

The order of introducing the solutions was from DI water to monotonically increasing concentrations of buffer, to avoid any errors due to fluid left over from higher concentration tested previously. For the nanogap sensor, a volume of 0.2 μl of each of the fluids was pipetted on to the sensor and the remaining fluid and the fluid from the cavities after taking the spectrum was removed using a small strip of lint-free absorbent paper. The buffers used were dilutions of SSC buffer, 0.15 M NaCl, 0.15 M sodium citrate, buffered to pH 6.8. The dilutions used were 1× SSC, 0.5× SSC, 0.2× SSC, 0.1× SSC, and 0.05× SSC. Using a reported pK_a of sodium citrate of 6.37 for the third ionization, we calculate

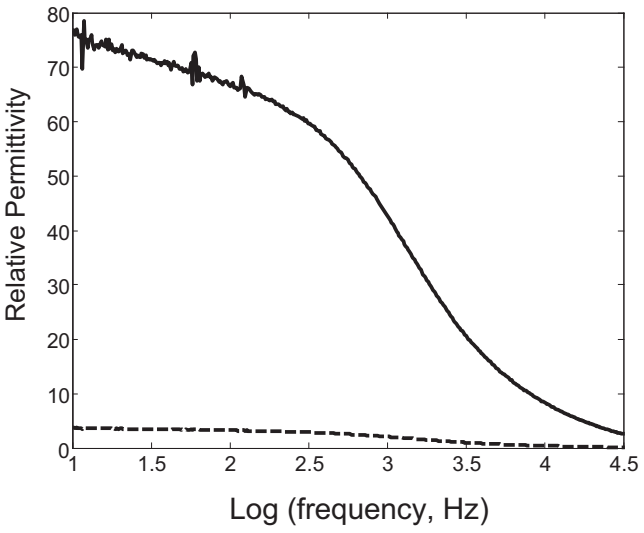

FIGURE 3 Dielectric spectrum of air (*dashed*) and DI water (*solid*) between the capacitive electrodes. The similarity in shape of the dielectric spectra of the DI water in the nanogap element to that of ice in a conventional capacitive element (29) suggests the ordering of the water molecules in the nanoscale confinement zone.

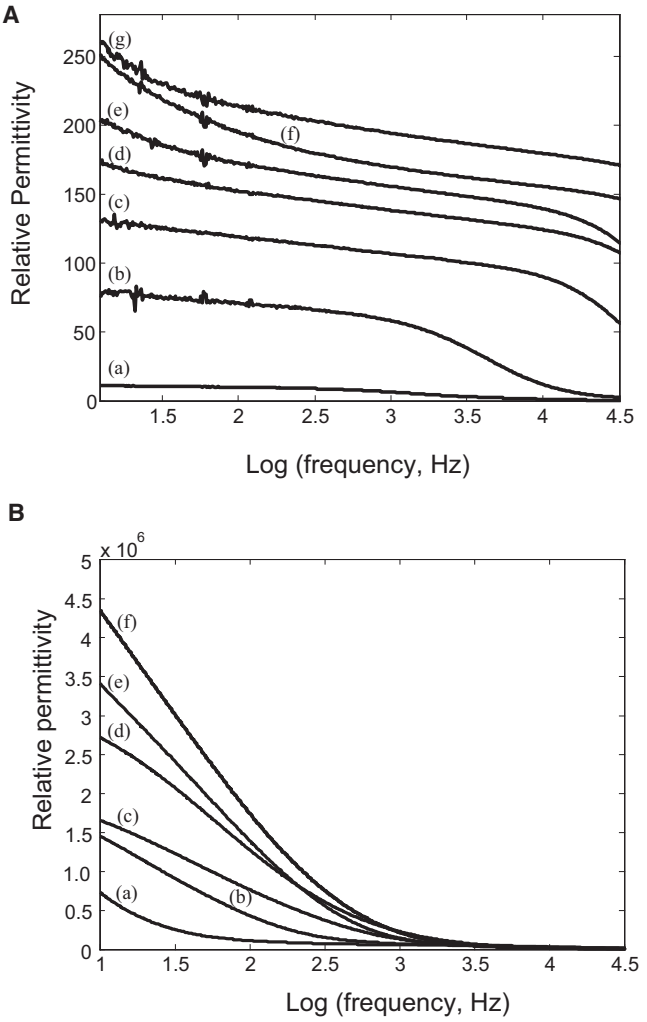

FIGURE 4 Relative permittivity as a function of frequency for various concentrations of buffer solutions obtained (*A*) using the nanogap capacitive element, and (*B*) using an interdigitated capacitive element with a gap size of 100 μm. The buffers used were dilutions of SSC buffer, 0.15 M NaCl, 0.015 M sodium citrate, buffered to pH 6.8. Plots (*a*) and (*b*) are for air and distilled water, respectively. The remaining plots are dilutions of SSC buffer: (*c*) 0.05× SSC, (*d*) 0.1× SSC, (*e*) 0.25× SSC, (*f*) 0.5× SSC, and (*g*) 1× SSC, with ionic strengths of 0.011 M, 0.023 M, 0.057 M, 0.114 M, and 0.227 M, respectively. All impedance measurements were carried out using an SR785 impedance analyzer. The high values of relative permittivities observed at low frequencies for the interdigitated element in *B* are attributed to the effect of electrode polarization. These relative permittivities are markedly reduced for the nanogap electrodes in *A*.

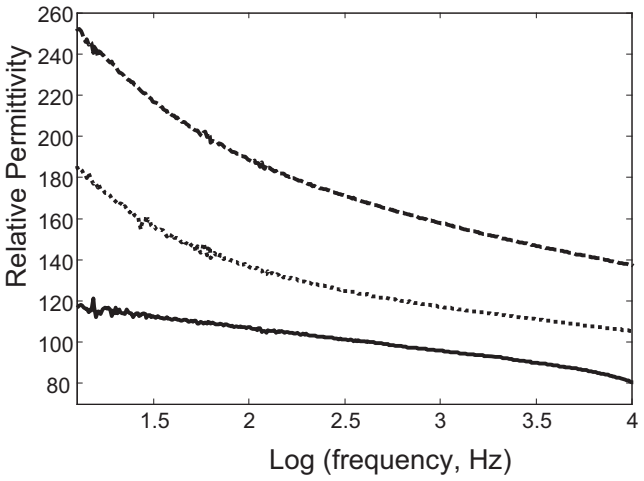

FIGURE 5 Dashed line shows the dielectric spectrum of a bare nanogap in the presence of 0.5× SSC buffer. The dotted curve shows the spectrum of the same nanogap after coating with a SAM of 100:1 mercaptohexanol/thio-derivatized aptamer. The solid curve shows the nanogap after SAM formation followed by α-thrombin binding. All the measurements were taken in 0.5× SSC buffer solution. The replacement of water molecules ($\varepsilon = 80$) by a monolayer of lower dielectric permittivity is reflected as a decrease in the overall sensor permittivity. The protein concentration in these experiments was 1 μM in 0.5× SSC buffer solution.

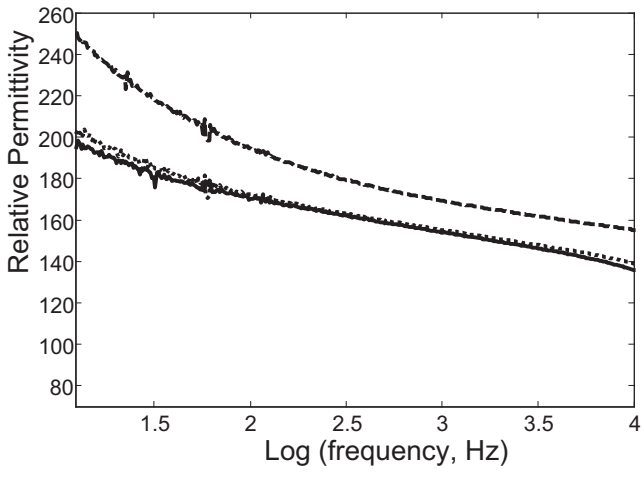

FIGURE 6 Dielectric spectrum of the interaction of (1 μM) lysozyme (*solid*) with the immobilized α-thrombin aptamer (*dotted*). The measurements were taken in 0.5× SSC buffer solution (*dashed*). The slight shift in the relative permittivity value can be explained by the nonspecific electrostatic binding between the positively charged protein molecules and the negatively charged aptamer sequences.

that at pH 6.8, the citrate ion is ~70% in the triply ionized state, and 30% in the doubly ionized state, which gives estimated ionic strengths of 0.227 M, 0.114 M, 0.057 M, 0.023 M, and 0.011 M, for these solutions, respectively.

The relative permittivity changes after aptamer immobilization and α-thrombin binding are shown in Fig. 5. As we can see, the immobilization of aptamer probes decreases the sensor permittivity significantly. The binding of protein molecules to the immobilized aptamers further enhances this effect. A dielectric spectrum of the interaction of the immobilized aptamer with lysozyme at the same concentration as the α-thrombin solution is shown in Fig. 6. The figure shows negligible changes in dielectric behavior on exposure to these nonspecific target molecules.

Dielectric spectra of the interaction of the α-thrombin molecules with a layer of immobilized control oligomer are shown in Fig. 7. This oligomer has the same nucleotide content (the same ratio of guanines to thymines) as the thrombin aptamer, but is unable to form the G-quadruplex structure responsible for specific binding. The figure shows negligible change in dielectric behavior on exposure to this nonspecific oligomer.

DISCUSSION

Relative permittivity versus frequency curves for pure water obtained using macroscale capacitors are dominated at low frequency by electrode polarization of dissolved hydroxyl and hydronium ions, leading to relative permittivity approaching 10^6 at 10 Hz. Only at frequencies approaching the kHz range do these parasitic effects diminish significantly, and the intrinsic relative permittivity of 80 is approached. In ionic solution, low-frequency Debye-layer contributions to the observed capacitance are even more dramatic, and highly salt-dependent, with relative permittivity at low frequencies in excess of 10^7 for ionic strengths of 0.01 M or higher (29). Hence, with conventional methods,

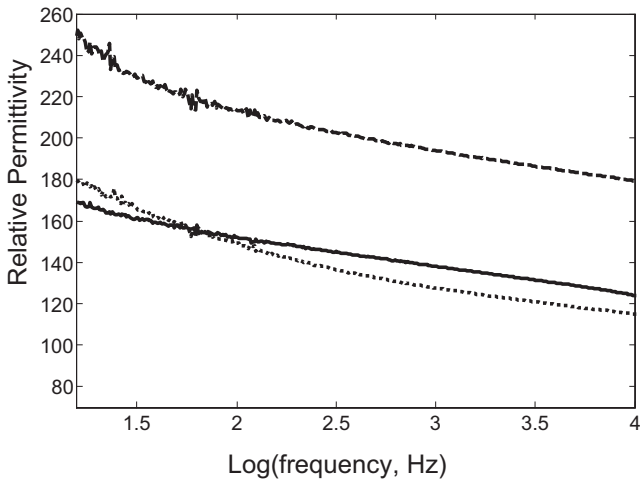

FIGURE 7 Dielectric spectra of a nanogap coated with a SAM containing immobilized control oligomer (incapable of forming the active G-quadruplex structure) in the absence (*dotted curve*) and presence (*solid curve*) of α-thrombin. The measurements were taken in 0.5× SSC buffer solution. The protein concentration was 1 μM. The nonspecific electrostatic binding between the positively charged protein molecules and the negatively charged oligonucleotide sequences can be observed as the slight shift in the relative permittivity. The dashed curve shows the permittivity of a solution of 0.5× SSC with no oligomer or protein present.

any low frequency contributions to the capacitance are swamped by parasitic contributions from ion gradient formation, and the observed permittivities are highly salt-dependent.

In contrast, the relative permittivity of water, measured by the nanogap sensor, is equal to the theoretical value of 80 at low frequency, diminishes in the kilohertz range, and approaches a higher frequency value of ~3. The curve that we obtain is similar in magnitude at low frequency, but not in frequency dependence, to the one presented by Yi et al. (17), for their nanogap sensors. In contrast to our results, these authors obtained curves that showed a large frequency dependence in the low-frequency range of 0–1000 Hz, whereas our data are relatively flat over this range. Also, these authors do not report data above 10 mM ionic strength, so a direct comparison can only be made under these low salt conditions. We believe that the differences between our results and those of Yi et al. (17), may reflect the fact that their nanogap electrodes were constructed using semiconductor electrodes made of doped silicon and polysilicon, whereas ours use conducting gold electrodes. Such different materials will both show different electrical properties and also (see below) differences in hydration.

Interestingly, our nanogap permittivity curves for pure water bear a close resemblance to curves that are typically obtained for ice (29). This observation may be fortuitous because for pure water the roughly micromolar concentrations of hydroxyl and hydronium ions give ionic gradients that extend well beyond the nanometer separations of the electrode, and hence should be effectively eliminated, even at low frequencies. On the other hand, it is anticipated that water confined within the volume of the nanogap may exist in a highly ordered form that is in many respects more ice-like than water-like. This hypothesis, although surprising at first glance, reflects a), the extraordinarily high surface/volume ratio of the confined water; and b), the natural tendency of water to order near interfaces.

As can be discerned from Fig. 4, both the absolute magnitude and the salt dependence of the relative permittivity of salt solutions are dramatically reduced at lower frequencies for the nanogap detector compared to conventional capacitive electrodes. Also, the nanogap curves are nearly constant over a wide frequency range, in dramatic contrast to the curves obtained for both conventional capacitive elements and for the semiconductor nanogap electrodes of Yi et al. (17). A partial understanding of these observations can be gleaned from Fig. 1, which shows theoretical calculations of ionic gradients for capacitive elements with various different ratios of gap distance to Debye length. Surprisingly, however, our nanogap element shows a dramatically reduced capacitance even at the highest salt concentration, compared to the interdigitated capacitor. In fact, the gap width should scarcely be relevant for the 1× SSC sample, because the effective Debye length under these circumstances is <1 nm. Nonetheless, the permittivities measured using the nanogap sensor for the 1× SSC solution are dramatically lower than the values obtained for the macroscale sensor. Although a definitive explanation of this result awaits further experimentation, we hypothesize that the high degree of order of water trapped within the confines of the nanogap limits the ability of ionic gradients to form on the timescale of the AC impedance measurements. Water ordering and release play a dominant role in interactions in aqueous solution not only for interactions involving hydrophobic interfaces, but for those involving hydrophilic interfaces as well (30). For example, DNA condensation seems to have a large attractive force related to water ordering from bound ions on DNA surfaces (31,32). Even a very hydrophilic surface such as gold can give short-range ordering of water at or near the gold-water interface. When water is trapped within a nanogap, a direct effect of water ordering could be a dielectric gradient near the electrode surfaces. Such water ordering could also markedly affect the water activity (or, equivalently, the osmotic pressure) within the nanogap region. A decrease in water activity could for example be compensated by a local decrease in ion concentration within the nanogap region. Effects such as these could significantly modify observed capacitive signals across the nanogap.

The approximations made in deriving the Poisson-Boltzmann equation include the assumption a mean field, the neglect of ion correlations, and the smearing of ionic charge. For the system under consideration here, the maximum AC voltage is 20 mV, and for a relative permittivity of 250, this corresponds to a measured capacitance of 4.4 pF. From the definition of capacitance, this implies a total charge on the 40 μm^2 surface of ~9×10^{-14} coulombs, or ~6×10^5 excess electrons per 40 μm^2. This result converts to ~70 nm^2 per excess electron. For this low surface charge density, these approximations seem very reasonable, and the Debye-Hückel approximation is entirely appropriate. Yet the nanogap capacitor outperforms the predictions of this elementary theory. At this stage in the development of the nanogap technology, we can only speculate as to the resolution of this (fortunate) discrepancy. Perhaps the resolution can be traced eventually to the assumption of a uniform dielectric. If there is indeed ordering of water within the very narrow nanogap then the assumption of a uniform dielectric is certainly not appropriate. Moreover, changes in water activity (osmotic pressure) could manifest in local deviations from the bulk ionic concentrations. In future work, it will be interesting to explore experimental measurements in mixed solvents and in the presence of divalent salts to test ideas such as these.

Regardless of the ultimate explanation for the reduced magnitude and salt-dependence of the relative permittivity for the nanogap compared to conventional capacitive elements, the net effect is that such sensors show a markedly reduced contribution from parasitic impedance at lower frequencies, suggesting an enhanced sensitivity to target-probe associations at these frequencies.

As we can see from Fig. 5, the immobilization of aptamer probes decreases the sensor permittivity, which can be explained by the replacement of water molecules of high relative permittivity ($\varepsilon = 80$) by biomolecules of low relative permittivity. The binding of protein molecules to the immobilized aptamers further enhances this effect. Dielectric spectra of the interaction of the immobilized aptamer with lysozyme at the same concentration as the α-thrombin solution are shown in Fig. 6. The figure shows negligible changes in dielectric behavior on exposure to these nonspecific target molecules. This result supports the relationship between capacitance (relative permittivity) change and specific biomolecular interaction.

Dielectric spectra of the interaction of the α-thrombin molecules with a layer of immobilized control oligomer are shown in Fig. 7. This oligomer is incapable of forming the G-quadruplex conformation to which α-thrombin specifically binds. The figure shows negligible change in dielectric behavior on exposure to these nonspecific target molecules. The slight shift in the relative permittivity in the case of both of these control experiments can be accounted for by the electrostatic interaction between the positively charged protein molecules (α-thrombin and lysozyme) and the negatively charged oligomers.

For a solution with 150 mM NaCl and 5 mM KCl, in 50 mM Tris buffer, the dissociation equilibrium constant of thrombin aptamer for thrombin has been determined as 20 nM by surface plasmon resonance (33). Under the lower salt conditions of the current measurements, even tighter binding is expected. In the experiments reported here, the nanogap element responds passively to target protein concentrations of 1 μM, in a total volume of 0.2 μL. At this high concentration, the nanogap should be fully saturated with bound thrombin. Now, in its current configuration, the nanogap sensor has dimensions of 1 μm $\times$ 40 μm and a gap separation of 20 nm, to give a total area of both Au electrodes that is on the order of 80 μm^2. If optimally coated, it is possible to obtain an active density of surface-attached DNA probe molecules on the order of 10^{12} mol/cm^2 (22). This density corresponds to a density of 10^4 mol/μm^2, or ~8×10^5 mol/sensor element. Now, because there are 6.02×10^5 mol/attomole, this corresponds to a conservative estimate of sensitivity in the attomole range, for a situation where all probe molecules are bound by target (saturation conditions). In fact, because our current methods of coating electrodes with probe molecules have not been optimized, it is possible that we may approach sensitivities in the zeptomole range. It remains to be determined how sensitive detection will be under target-limited conditions.

We believe that the results that we have presented show that nanogap capacitive sensors can specifically detect target molecules even under physiologically relevant ionic strength conditions. A key challenge for future work will be to develop the technology to a stage where it can be used to obtain equilibrium binding constants and potentially kinetic information as well. Such work is currently under way in our laboratory.

CONCLUSION

In this study, we have demonstrated the use of nanogap dielectric sensors for attaining highly sensitive, label-free detection of α-thrombin using immobilized aptamer probes. Control experiments show that the method clearly distinguishes specific binding between α-thrombin and its cognate aptamer from nonspecific interactions between thrombin and nonaptamer oligonucleotides. Additional control measurements demonstrate that the method also distinguishes specific aptamer binding from the nonspecific interaction between the acidic protein lysozyme and the thrombin aptamer. The nano scale space confinement of capacitive electrodes is shown to eliminate noise from electrode polarization effects and solution conductivity, thereby permitting dielectric spectroscopic measurements at low frequencies. The increased sensitivity demonstrated by these molecular scale sensors combined with the use of reduced sample volume, label-free operation, and the improvement in shelf life due to the use of immobilized aptamers are promising for applications such as point of care diagnostics using low-cost, portable, hand-held diagnostic tools.

The devices were fabricated in the New Jersey Institute of Technology Microelectronics Fabrication Center clean rooms. We express our gratitude to Dr. Rajendra K. Jarwal of the Microelectronics Fabrication Center for assistance in the fabrication procedures and for many key discussions.

William Braunlin and Les Beadling are cofounders of Rational Affinity Devices. Manu Sebastian Mannoor, Dentcho V. Ivanov, and Teena James are consultants and technical advisors to Rational Affinity Devices.

REFERENCES

1. Herick, K., P. Jackson, …, A. Burkovski. 2001. Detection of fluorescence dye-labeled proteins in 2-D gels using an Arthur 1442 Multiwavelength Fluoro imager. *Biotechniques.* 31:146–149.
2. Cao, Z., Z. Li, …, J. Lu. 2006. Magnetic bead-based chemiluminescence detection of sequence-specific DNA by using catalytic nucleic acid labels. *Anal. Chim. Acta.* 557:152–158.
3. Schlensog, M. D., T. M. A. Gronewold, …, E. Quandt. 2004. A Lovewave biosensor using nucleic acids as ligands. *Sens. Actuators B Chem.* 101:308–315.
4. Berggren, C., B. Bjarnason, and G. Johansson. 2001. Capacitive biosensors. *Electroanalysis.* 13:173–180.
5. Loehndorf, M., U. Schlecht, …, M. Tewes. 2005. Microfabricated high-performance microwave impedance biosensors for detection of aptamer-protein interactions. *Appl. Phys. Lett.* 87:243902.
6. Takashima, S. 1989. Electrical Properties of Biopolymers and Membranes. Taylor & Francis, London.
7. Grant, E. H., R. J. Sheppard, and G. P. South. 1978. Dielectric Behaviour of Biological Molecules in Solution. Oxford University Press, Oxford.
8. Baker-Jarvis, J., C. A. Jones, and B. Riddle. 1998. Electrical properties and dielectric relaxation of DNA in solution. NIST Technical Note:1509.
9. Mandel, M. 1977. Dielectric properties of charged linear macromolecules with particular reference to DNA. *Ann. N. Y. Acad. Sci.* 303:74–89.

10. Saif, B., R. K. Mohr, …, T. A. Litovitz. 1991. On the mechanism of dielectric relaxation in aqueous DNA solutions. *Biopolymers.* 31:1171–1180.

11. Takashima, S. 1967. Effect of ions on the dielectric relaxation of DNA. *Biopolymers.* 5:899–913.

12. van der Touw, F., and M. Mandel. 1974. Dielectric increment and dielectric dispersion of solutions containing simple charged linear macromolecules. I. Theory. *Biophys. Chem.* 2:218–230.

13. Sanabria, H., and J. H. Miller. 2006. Relaxation processes due to the electrode-electrolyte interface in ionic solutions. *Phys. Rev. E.* 74:051505.

14. Oleinikova, A., P. Sasisanker, and H. Weingärtner. 2004. What can really be learned from dielectric spectroscopy of protein solutions? A case study of ribonuclease A. *J. Phys. Chem. B.* 108:8467–8474.

15. Schwan, H. P. 1993-1994. Mechanisms responsible for electrical properties of tissues and cell suspensions. *Med. Prog. Technol.* 19:163–165.

16. Fricke, H., and H. J. Curtis. 1937. The dielectric properties of water-dielectric interphases. *J. Phys. Chem.* 41:729–745.

17. Yi, M., K. H. Jeong, and L. P. Lee. 2005. Theoretical and experimental study towards a nanogap dielectric biosensor. *Biosens. Bioelectron.* 20:1320–1326.

18. Morgan, C. L., D. J. Newman, and C. P. Price. 1996. Immunosensors: technology and opportunities in laboratory medicine. *Clin. Chem.* 42:193–209.

19. Tom-Moy, M., R. L. Baer, …, T. P. Doherty. 1995. Atrazine measurements using surface transverse wave devices. *Anal. Chem.* 67:1510–1516.

20. Zuo, X., Y. Xiao, and K. W. Plaxco. 2009. High specificity, electrochemical sandwich assays based on single aptamer sequences and suitable for the direct detection of small-molecule targets in blood and other complex matrices. *J. Am. Chem. Soc.* 131:6944–6945.

21. Yao, C., Y. Qi, …, W. Fu. 2009. Aptamer-based piezoelectric quartz crystal microbalance biosensor array for the quantification of IgE. *Biosens. Bioelectron.* 24:2499–2503.

22. Beaucage, S. L. 2001. Strategies in the preparation of DNA oligonucleotide arrays for diagnostic applications. *Curr. Med. Chem.* 8:1213–1244.

23. Macaya, R. F., P. Schultze, …, J. Feigon. 1993. Thrombin-binding DNA aptamer forms a unimolecular quadruplex structure in solution. *Proc. Natl. Acad. Sci. USA.* 90:3745–3749.

24. Padmanabhan, K., K. P. Padmanabhan, …, A. Tulinsky. 1993. The structure of alpha-thrombin inhibited by a 15-mer single-stranded DNA aptamer. *J. Biol. Chem.* 268:17651–17654.

25. Wang, K. Y., S. McCurdy, …, P. H. Bolton. 1993. A DNA aptamer which binds to and inhibits thrombin exhibits a new structural motif for DNA. *Biochemistry.* 32:1899–1904.

26. Verwey, E. J. W. 1935. The electrical double layer and the stability of lyophobic colloids. I. The electrical double layer. *Chem. Rev.* 16:363–415.

27. Verwey, E. J. W., and J. T. G. Overbeek. 1948. Theory of the Stability of Lyophobic Colloids. Elsevier, New York.

28. Nuzzo, R. G., and D. L. Allara. 1983. Adsorption of bifunctional organic disulfides on gold surfaces. *J. Am. Chem. Soc.* 105:4481–4483.

29. Seshadri, S., K. B. Chin, …, R. C. Anderson. 2008. Using electrical impedance spectroscopy to detect water in planetary regoliths. *Astrobiology.* 8:781–792.

30. Parsegian, V. A., R. P. Rand, and D. C. Rau. 2000. Osmotic stress, crowding, preferential hydration, and binding: A comparison of perspectives. *Proc. Natl. Acad. Sci. USA.* 97:3987–3992.

31. Rau, D. C., and V. A. Parsegian. 1992. Direct measurement of the intermolecular forces between counterion-condensed DNA double helices. Evidence for long range attractive hydration forces. *Biophys. J.* 61:246–259.

32. Todd, B. A., V. A. Parsegian, …, D. C. Rau. 2008. Attractive forces between cation condensed DNA double helices. *Biophys. J.* 94:4775–4782.

33. Hasegawa, H., K. Taira, …, K. Ikebukuro. 2008. Improvement of aptamer affinity by dimerization. *Sensors.* 8:1090–1098.